Supporting Information

Combining IL-2-based Immunotherapy with Commensal Probiotics Produces Enhanced Antitumor Immune Response and Tumor Clearance

Linlin Shi[1†], Jianyong Sheng[1†], Guozhong Chen[2], Peng Zhu[3], Changping Shi[2], Bei Li[2], Chaiwoo Park[2], Jingyi Wang[4], Bixiang Zhang[3*], Zhi Liu[2*] and Xiangliang Yang[1*]

[1]National Engineering Research Center for Nanomedicine, College of Life Science and Technology, Huazhong University of Science and Technology, Wuhan, China

[2]Department of Biotechnology, College of Life Science and Technology, Huazhong University of Science and Technology, Wuhan, China

[3]Hepatic Surgery Center, Tongji Hospital, Tongji Medical College, Huazhong University of Science and Technology, Wuhan, China

[4]Department of Biology, St. Olaf College, Minnesota, USA

[†] These author contributed equally to this work.

* Correspondence: bixiangzhang@163.com; zhiliu@hust.edu.cn; yangxl@hust.edu.cn

Inventory

Supplementary Materials and Methods

35 Supplementary Figures

1 Supplementary Table

Supplementary Materials and Methods

Flow cytometry analysis of CRC patients derived tumor tissues

Tumor tissues collected from CRC patients were cut into small pieces and digested and filtered into single cell suspensions. For cell viability analysis, IL-2 and AKK were prepared and added to the cultured cells from CRC patients. The cells were observed under a microscope every six hours. After cultured for 24 hours, cells were collected and stained with annexin V and propidiumiodide for apoptosis detection by flow cytometry. For tumor immune microenvironment analysis, single cell suspensions of tumor infiltrating lymphocytes were isolated from CRC patients and treated with IL-2, AKK and their combined therapy for 24h. For cell surface staining, the suspensions were incubated with FITC-labeled anti-human CD3 antibody (clone HIT3a, cat. 300306), PerCP/Cy5.5-labeled anti-human CD4 antibody (clone RPA-T4, cat. 300529) and PE-labeled anti-human CD8a antibody (clone RPA-T8, cat. 301008). For intracellular cytokine staining, lymphocytes prepared from tumor mass were restimulated using phorbol 12-myristate 13-acetate (PMA; 50 ng/mL) and ionomycin (1mg/mL; Sigma-Aldrich) in the presence of Brefeldin A (1 mg/mL; eBioscience) for 4h. Subsequently, the simulated lymphocytes were stained with FITC-labeled anti-mouse CD3 antibody and PE-labeled anti-human CD8a antibody as described above. After surface staining, cells were treated with Fix/Perm solution and restained with APC anti-human IFN-γ antibody (clone 4S.B3, cat. 502511). For dendritic cell analysis, tumor infiltrating lymphocytes were stained with APC-labeled anti-human CD11c antibody (clone 3.9, cat. 301613), PE-labeled anti-human I-A/I-E antibody (clone L243, cat. 307605), FITC-labeled anti-human CD80 antibody (clone 2D10, cat. 305205) and PerCP/Cy5.5-labeled anti-human CD86 antibody (clone IT2.2, cat. 305419).

Flow cytometry analysis of tumor-bearing mice derived tumor tissues

Tumor tissues were isolated from subcutaneous tumor bearing mice, digested by collagenase and filtered into single cell suspensions. Afterward, the suspensions were stained with FITC-labeled anti-mouse CD3 antibody (clone 145-2C11, cat. 100203), PerCP/Cy5.5-labeled anti-mouse CD4 antibody (clone GK1.5, cat. 100434) and APC-labeled anti-mouse CD8a antibody (clone 53-6.7, cat. 100712). For intracellular cytokine staining, single cell suspensions prepared from tumor infiltrating lymph node were restimulated using phorbol 12-myristate 13-acetate (PMA; 50 ng/mL) and ionomycin (1mg/mL; Sigma-Aldrich) in the presence of Brefeldin A (1 mg/ml; eBioscience) for 4h. Subsequently, the simulated lymphocytes were stained with FITC-labeled anti-mouse CD3 antibody and APC-labeled anti-mouse CD8a antibody as described above. After surface staining, cells were treated with Fix/Perm solution and restained with PE-labeled anti-mouse IFN-γ antibody (clone XMG1.2, cat. 505807). For nuclear transcription factor staining, tumor infiltrating lymphocyte were stained with PerCP/Cy5.5-labeled anti-mouse CD4 antibody and APC-labeled anti-mouse CD25 antibody (clone PC 61, cat. 102011). Afterwards, cells were incubated with Fix/Perm solution and restained with PE-labeled anti-mouse Foxp3 antibody (clone MF-14, cat. 126403). For dendritic cell analysis, tumor infiltrating lymphocytes were stained with FITC-labeled anti-mouse CD11c antibody (clone N418, cat. 117305), PE/Cy7-labeled anti-mouse I-A/I-E antibody (clone M5/114.15.2, cat. 107629), PE-labeled anti-mouse CD80 antibody (clone 16-10A1, cat. 104707) and APC-labeled anti-mouse CD86 antibody (clone GL-1, cat. 105011). All antibodies were purchased from BioLegend (San Diego, USA), and flow cytometric analysis was performed by using a CytoFlex flow cytometry system (Beckman Coulter, USA).

Flow cytometry analysis of side population cells

1×10^6 single cell suspensions in culture medium containing 1 % FBS were prepared from tumor tissues of subcutaneous tumor bearing mice. The suspensions were stained with fluorescent dye (Hoechst 33342) at 5 μg/mL in the presence or absence of 50 μM verapamil. Then, cells were

incubated in darkness at 37 °C for 90 min, washed twice with pre-cooling PBS and resuspended in 300 μL PBS and kept on ice until further analysis.

Tumor-repopulating cells culture

Tumor-repopulating cells were selected from the single cell suspensions by soft 3D fibrin gels according to the previous study [1]. First, fibrinogen was diluted to 2 mg/mL with T7 buffer (50 mM Tris, pH 7.4, 150 mM NaCl). Fibrinogen/cell mixtures were obtained by blending 2 mg/mL fibrinogen with similar volume of cell suspension (2×10^3 cells/mL), which produced gels of 90 Pa in elastic stiffness. 250 μL of the mixtures were loaded into each well of 24-well plate pre-added with 5 μL thrombin (0.1 U/μL). The cell culture plate was then incubated at 37 °C for 30 min. Finally, 1 ml RPMI 1640 medium containing 10 % FBS and antibiotics were added. On the fifth day, tumor spheroids were obtained, and the colony size and number were measured.

Antitumor effect and mechanism study of Amuc in tumor bearing mice

To explore the involvement of TLR2 pathway in the antitumor effects of Amuc, tumor-bearing mice received i.p. injection of BLP at 10 μg per mice and CU-CPT22 at 3 mg/kg every 5 days for 3 weeks. Amuc was delivered at 10 μg per mice by oral administration every three days for 3 weeks. Tumor volume and body weight were recorded every 3 days. The length (L) and width (W) of tumor were measured every other day with a digital caliper and tumor volume was calculated as $L\times W^2\times0.5$. When the tumor volume reached about 2000 mm^3, mice were sacrificed according to the guidelines for animal care. Tumor samples were collected for further analysis. All mice received the humane care and had free access to water and the maintenance diet.

Dual-luciferase reporter gene assay for TLR2

Human HEK 293T cells were seeded at a density of 1×10^5 cells in 24-well plates. Cells were transfected with 1μg PCDNA3.1(+)-hTLR2-Flag plasmid, 0.5 μg pGL4.32-NF-κB-luciferase

plasmid, and 0.01 ug pRL-TK plasmid by using Lipofectamine 2000 reagent (Invitrogen). After incubation for 24 h, the transfection solutions were replaced with AKK suspension (1×10^7 CFU/mL) or Amuc solution (10 μg/mL), followed by incubation at 37 °C in a 5% CO_2 incubator for 24 h. Receptor ligand Pam3CSK4 (10 ng/mL) and maintenance medium (DMEM) were used as the positive control and the negative control, respectively. Subsequently, cells were rinsed twice with PBS (pH 7.4) and lysed with 1× passive lysis buffer (100 μL/well). The Luciferase and Renilla luciferase activity were separately measured using a fluorescence spectrophotometer (GloMax® 20/20 Luminometer, Promega) following the manufacturer's instructions for the Dual-Luciferase Assay System (Promega). The activation ratio of TLR2/ NF-κB was calculated by fluorescent detection to evaluate the level of TLR2 activation.

AKK detection in vivo

Fecal samples, intestinal contents and tumor tissues were collected from saline treated tumor bearing mice and AKK treated mice. Total genomic DNA from the obtained samples were extracted by QIAamp DNA Stool Mini Kit and QIAamp Fast DNA Tissue Kit (QIAGEN, Germany) according to the manufacturer's guide. Specific primer sequences for the detection of AKK were chosen from the previous methods [2]. Samples were subjected to 35 cycles of amplification. Preincubation was for 5 min at 95 °C, followed by 35 cycles of 30 s at 95 °C, 30s at 54 °C, and 30 s at 72 °C. PCR products in each group were visualized by agarose gel electrophoresis following the standard protocols.

Microbial DNA extraction and sequencing

Mice fecal samples were frozen at -80 °C immediately after collection. Total genomic DNA from around 200 mg of stool was extracted by QIAamp DNA Stool Mini Kit (QIAGEN, Germany) according to the manufacturer's guide. The V3-V4 region of the bacterial 16S ribosomal RNA (rRNA) genes was amplified by PCR with universal primer sequences (338F, ACTCCTACGGGAGGCAGCAG; 806R, GGACTACHVGGGTWTCTAAT) and FastPfu Polymerase. Amplicons were then purified by gel extraction (AxyPrep DNA GelExtraction Kit,

Axygen Biosciences, USA) and were quantified using QuantiFluor-ST (Promega, USA). The purified amplicons were pooled in equimolar concentrations, and paired-end sequencing was performed using an Illumina MiSeq platform (Illumina, San Diego, USA).

Expression and purification of AKK-derived outer membrane protein

The outer membrane protein of AKK (here termed Amuc) was expressed and purified following the previous method with modifications [3]. The expression plasmid was constructed by amplification of its gene devoid of the coding sequence for its signal sequence and cloning of the resulting PCR product in pET28a-Amuc.

The resulted plasmid pET28a-Amuc, with the conformation confirmed by sequence analysis, was transformed into *E. coli* BL21. This strain was then grown in LB-broth containing kanamycin (50 μg/mL) followed by IPTG induction at a final concentration of 2 mM by shaking at 220 rpm at 28 °C. After ten hours of induction, cells were pelleted by centrifugation at 9,000 g for 15 min and stored at -80 °C for further lysis. Cell pellets were resuspended and lysed using lysozyme and ultrasonic homogenizer (SCIENTZ, Ningbo, China). After centrifugation, the supernatants were collected and purified for Amuc by using BeyoGold™ His-tag Purification Resin (Beyotime, Shanghai, China). The purified protein sample was determined by BCA assay and stored at -80 °C for further experiments.

RNA sequencing and data analysis

Total RNAs were prepared with Trizol reagent (Invitrogen, USA) and were sequenced by Illumina HiSeq X10 (Illumina, USA). Significance analysis (2-fold change and P-value < 0.05) was used to identify the differential genes with a false discovery rate (FDR) < 0.05. All identified sequences were mapped with Gene Ontology Terms (GO, http://geneontology.org/) and Kyoto Encyclopedia of Genes and Genomes (KEGG, https://www.kegg.jp/) to determine the functional and biological properties. Hypergeometric test was employed to conduct GO and KEGG pathway enrichment.

Preparation and purification of antibodies against Amuc

Polyclonal-antibodies against Amuc were prepared by Dia-An Biotech, China. 2 mg of purified Amuc protein was mixed with FCA (Freund's complete adjuvant) or FIA (Freund's incomplete adjuvant), followed by subcutaneous injection into two Japanese white rabbits for four times. The mixture containing FCA was only used in the first injection, while the mixture with FIA for the rest three injections. The 2nd injection was on the 28th day post the first injection. There were 2-week intervals between other injections. On the third day after the last injection, antiserum titer was tested by ELISA. On the 64th day post the first injection, the rabbits with higher titer was killed and its blood was collected. An affinity column for the purification of the antibodies was made by coupling 1mg purified Amuc protein to CNBr-activated Sepharose 4B from GE. The antiserum was applied onto the column, followed by elution of the specific antibodies using the Glycine HCl buffer at pH 2.5.

Culture and in vitro activation of BMDC

To prepare bone marrow-derived dendritic cells (BMDCs), the tibias and femurs of normal C57BL/6 mice (wt) were removed under sterile conditions. Bone marrow cells were flushed out from the bone cavity gently using the needle of a 1 mL syringe and then inserted into a sterile culture dish with RPMI-1640 medium. Cell suspensions in the dish were centrifuged at 1200 rpm for 5 min and resuspended in RPMI-1640 medium supplemented with 10% FBS, 10 ng/mL IL-4 and 20 ng/mL GM-CSF. Cell were then distributed into 24-well plates (NEST Biotechnology, Wuxi, China) at a density of 1×10^6 cell/mL and were cultured for 5 days in 37 °C, 5 % CO_2. On day 3, a fresh cell culture medium containing IL-4 and GM-CSF were added. On day 5, the nonadherent cells suspended in the medium were collected, centrifuged, and resuspended in the fresh culture medium containing IL-4 and GM-CSF. For further activation, 1×10^6 BMDCs were seeded in a 6-well plate (NEST Biotechnology, Wuxi, China) and stimulated with PBS, Amuc (10 μg/mL), and AKK (1×10^7 CFU/mL) for 24 h. The expression of the surface markers CD11c, MHC-II, and CD86 on the BMDCs was then measured and calculated by flow cytometry.

Histological analysis

Tumor tissues were fixed in 4 % paraformaldehyde, sectioned and stained with H&E. The rest of tumor tissues were frozen and prepared to be stained with Ki67 and TUNEL according to the manufacturer's instructions. Cell nuclei were stained by DAPI. For immunofluorescence staining of CD133, frozen slices of the dissected tumor tissues from different groups were blocked with 5% BSA in PBS for 60 min. Heat mediated antigen retrieval was performed in 0.01M citrate-buffer (pH 6.0). The slices were then incubated with a 1:500 dilution of anti-CD133 antibody (ab19898, Abcam, USA) and rocked on an orbital shaker (Mini Roller, NEST Biotechnology, China) at 4°C in the dark overnight. Afterwards the tumor slices were treated with CY3-conjugated goat anti-rabbit antibody (GB21303, Servicebio, China), the secondary antibody, in PBS at room temperature in the dark for 60 min. Cell nuclei were stained with DAPI (Sigma, USA). Stained cells were then visualized by fluorescence microscopy (Nikon Eclipse CI, Japan). Images were acquired with Nikon digital sight DS-Fi2 imaging system (exposure time: 10 ms for DAPI and 80 ms for CY3, at 200× magnification) under the same acquisition settings throughout image capturing. The positively stained cells were recorded from three visual fields at 200× magnification per slice. The average percentage of $CD133^+$ cells was processed using Image Pro Plus 6.0 (Media Cybernetics, USA).

Intestinal samples of mice were fixed in 4 % paraformaldehyde at room temperature overnight and then embedded in paraffin. Tissues were sectioned at 5 μm thickness and dipped in hematoxylin and eosin (H&E) using standard protocols. For AB-PAS staining, the mice intestinal samples were fixed in Carnoy's Fluid. Dewaxed sections were hydrated and stained with Alcian blue for 5-10 min followed by treatment with periodic acid for 10-15 min. Then, sections were stained with Schiff's reagent for 15-30 min in the darkness, washed in running tap water for 5-10 min and dehydrated in gradient alcohol before mounting with neutral gum. For immunofluorescent staining of mucus layer, intestinal samples of mice were stained with

Mucin2 (Santa Cruz Biotechnology, USA) following the standard procedures. Images of the stained sections were acquired by fluorescence microscopy (Nikon Eclipse CI, Japan).

References

1. Liu J, Tan Y, Zhang H, Zhang Y, Xu P, Chen J, Poh YC, Tang K, Wang N, Huang B. Soft fibrin gels promote selection and growth of tumorigenic cells. Nat Mater. 2012;11:734-41.
2. Collado MC, Derrien M, Isolauri E, de Vos WM, Salminen S. Intestinal integrity and Akkermansia muciniphila, a mucin-degrading member of the intestinal microbiota present in infants, adults, and the elderly. Appl Environ Microbiol. 2007; 73:7767-70.
3. Plovier H, Everard A, Druart C, Depommier C, Van Hul M, Geurts L, Chilloux J, Ottman N, Duparc T, Lichtenstein L, et al. A purified membrane protein from Akkermansia muciniphila or the pasteurized bacterium improves metabolism in obese and diabetic mice. Nat Med. 2017; 23:107-113.

Supplementary Figures

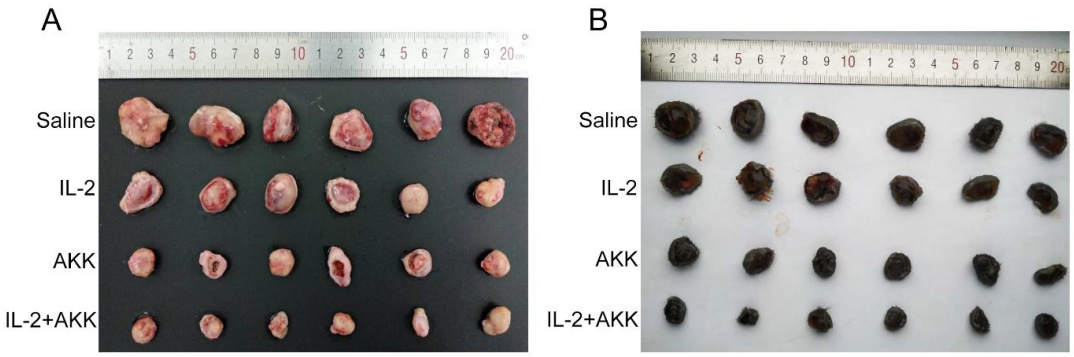

Figure S1. Antitumor effect of combination therapy of IL-2 and AKK in tumor bearing mice. Images of tumor tissues isolated from CT26 tumor-bearing mice (A) or B16F10 tumor-bearing mice (B) at the end of the experiment (n = 6).

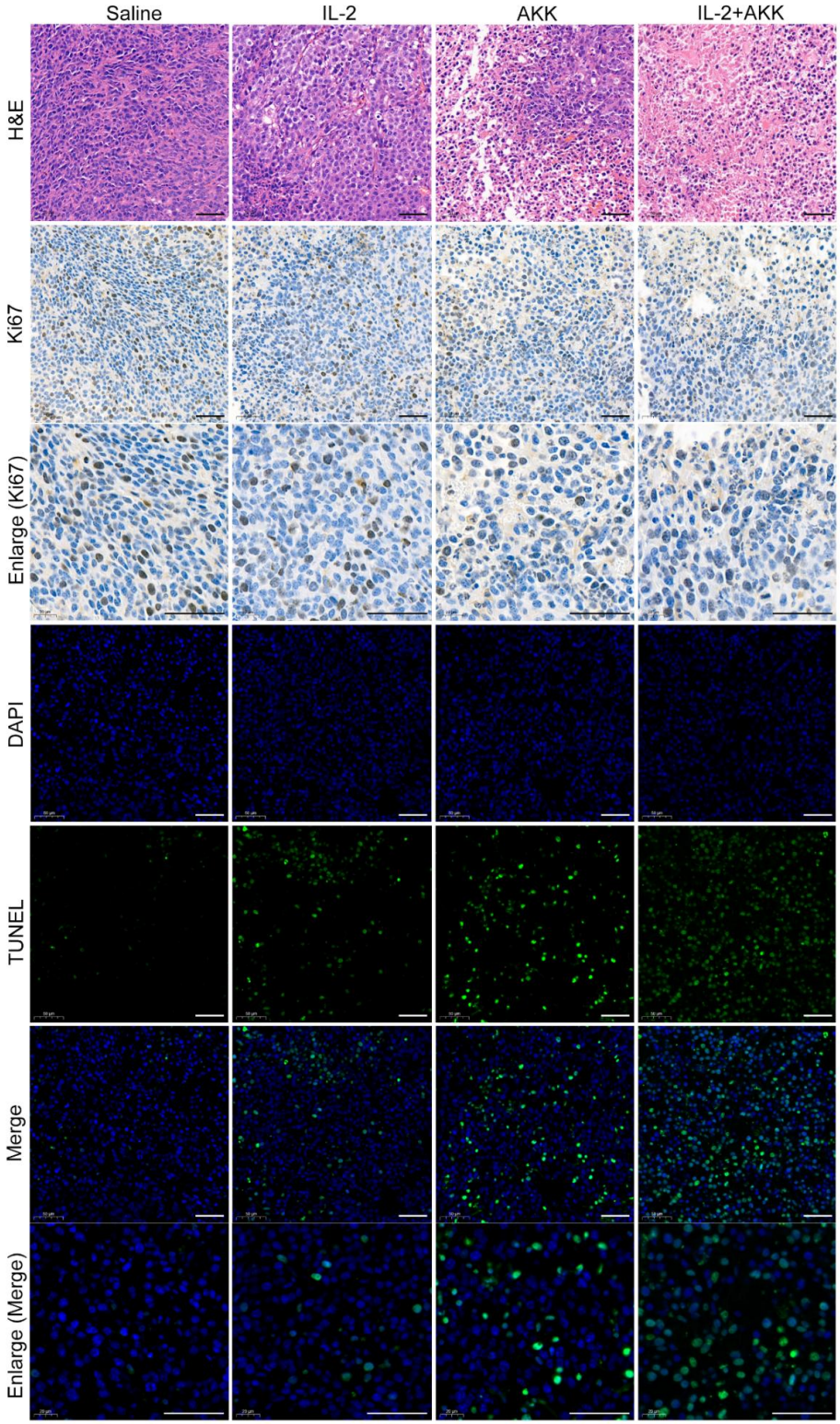

Figure S2. Representative histological staining of tumor sections from CT26 tumor-bearing mice at the end of the experiment (200× or 400× enlargement, scale bar = 50 μm).

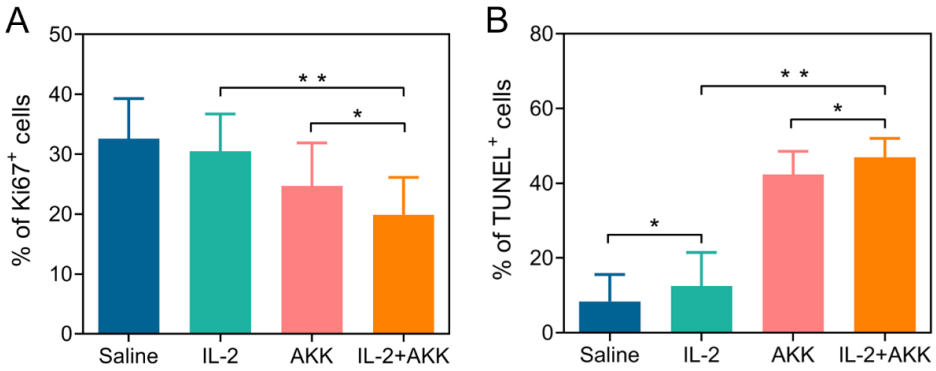

Figure S3. Quantitative analysis of Ki67$^+$ cells (A) and TUNEL$^+$ cells (B) in the tumor tissues collected from CT26 tumor bearing mice among different treatment groups (n = 6). All data are shown as mean ± SD (*$P < 0.05$, ** $P < 0.01$).

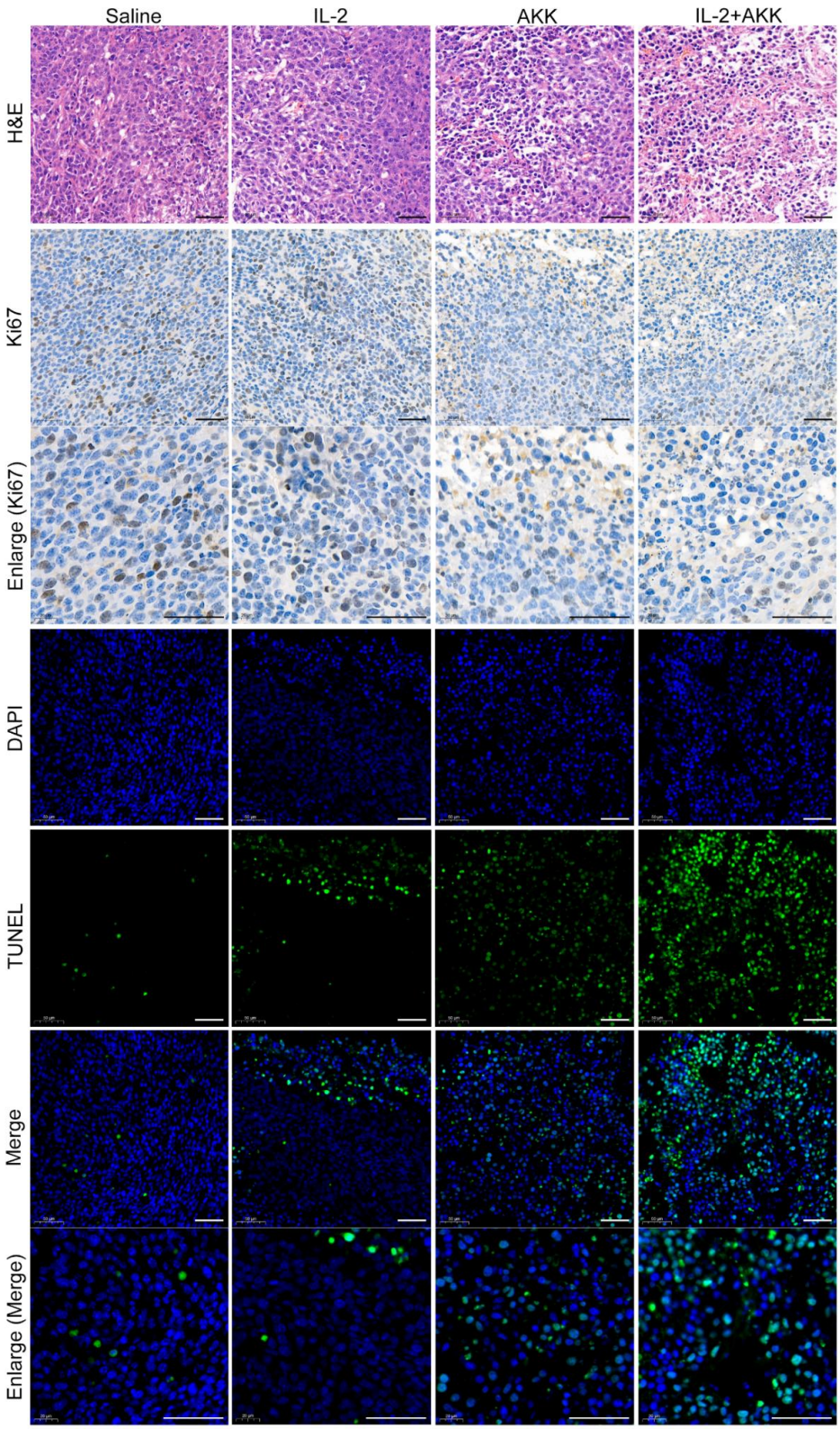

Figure S4. Representative histological staining of tumor sections from B16F10 tumor-bearing mice at the end of the experiment (200× or 400× enlargement, scale bar = 50 μm).

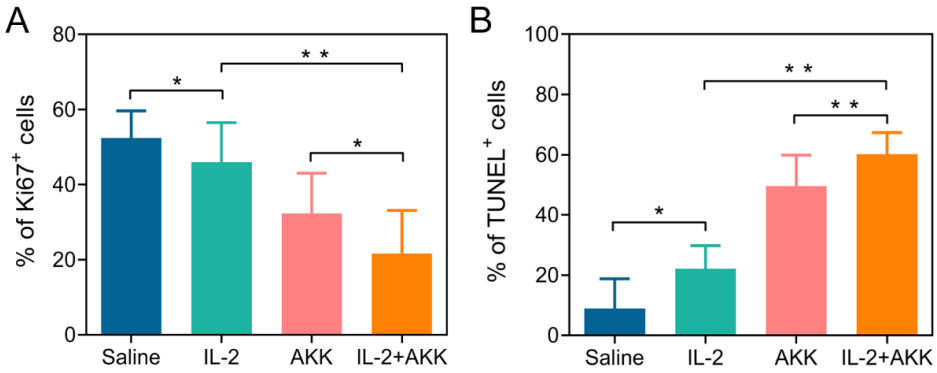

Figure S5. Quantitative analysis of Ki67⁺ cells (A) and TUNEL⁺ cells (B) in the tumor tissues collected from B16F10 tumor bearing mice among different treatment groups (n = 6). All data are shown as mean ± SD (*$P < 0.05$, ** $P < 0.01$).

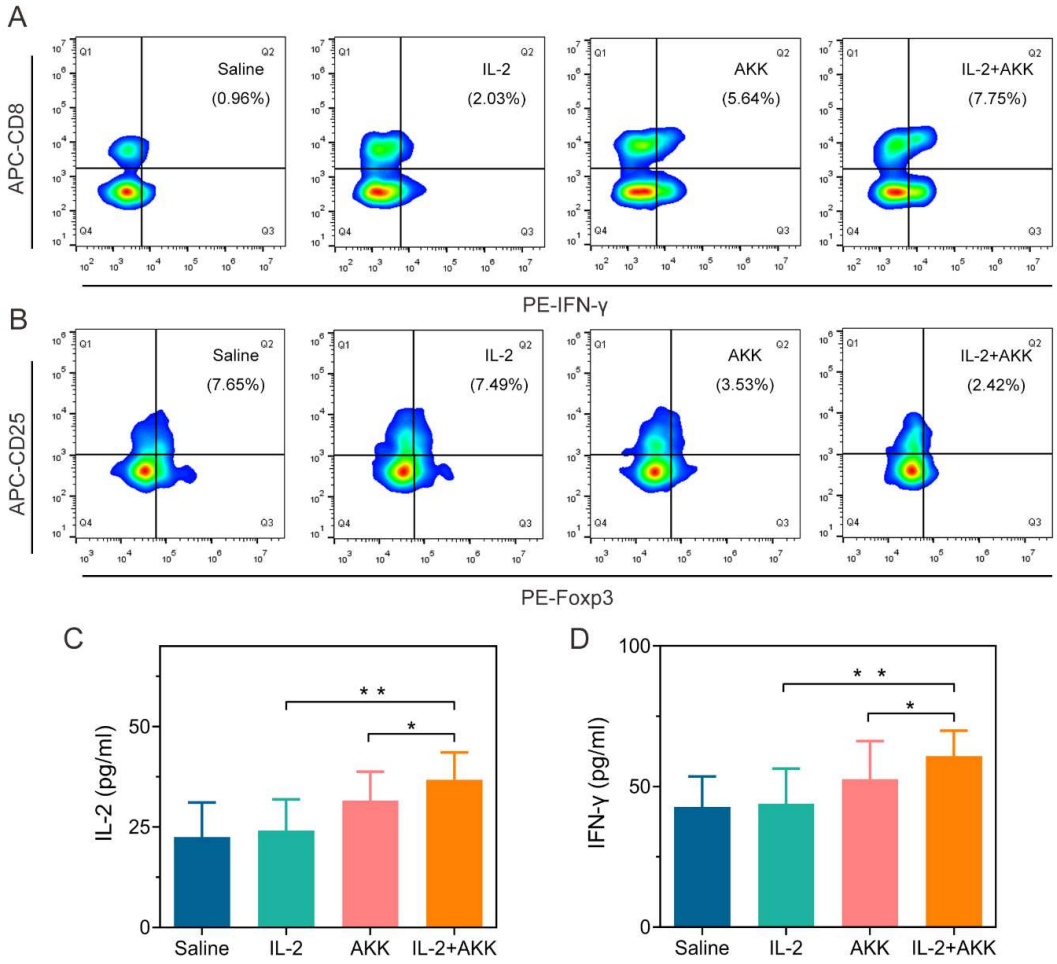

Figure S6. Alterations of tumor immune microenvironment in B16F10 tumor-bearing mice under combination therapy of IL-2 and AKK. (A) Representative flow cytometry analysis of CTLs in tumor-draining lymph nodes. (B) Representative flow cytometry analysis of Tregs in tumor-draining lymph nodes. (C, D) ELISA measurement of IL-2 (C) and IFN-γ (D) in the homogenates of tumor tissues among different groups. All data are shown as mean ± SD (n = 6, **P* < 0.05, ** *P* < 0.01).

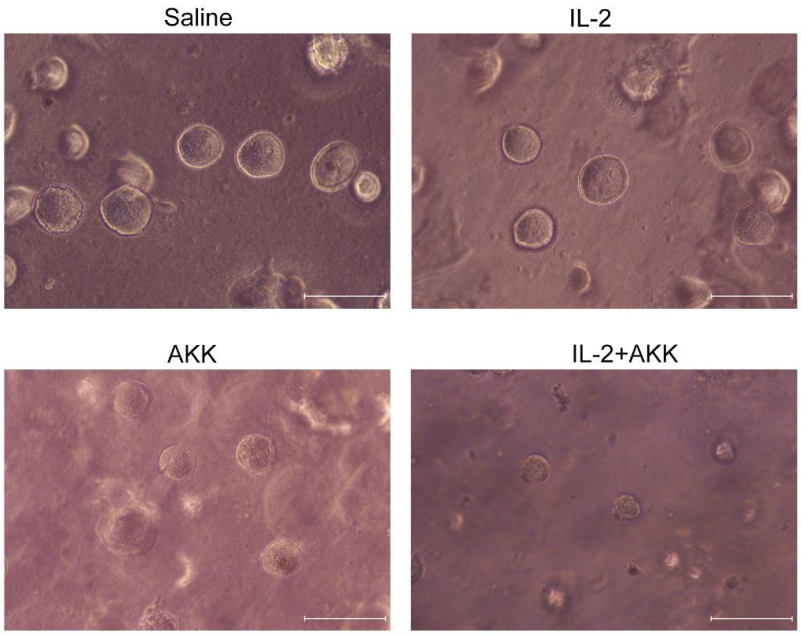

Figure S7. Representative images of tumor spheroids from CT26 tumor-bearing mice under different treatments. Tumor tissues were collected from CT26 tumor-bearing mice among different groups. Single cell suspensions were prepared from the tumor tissues, and then were seeded into soft 3D fibrin gels and incubated for 5 days. Scale bar = 50 μm.

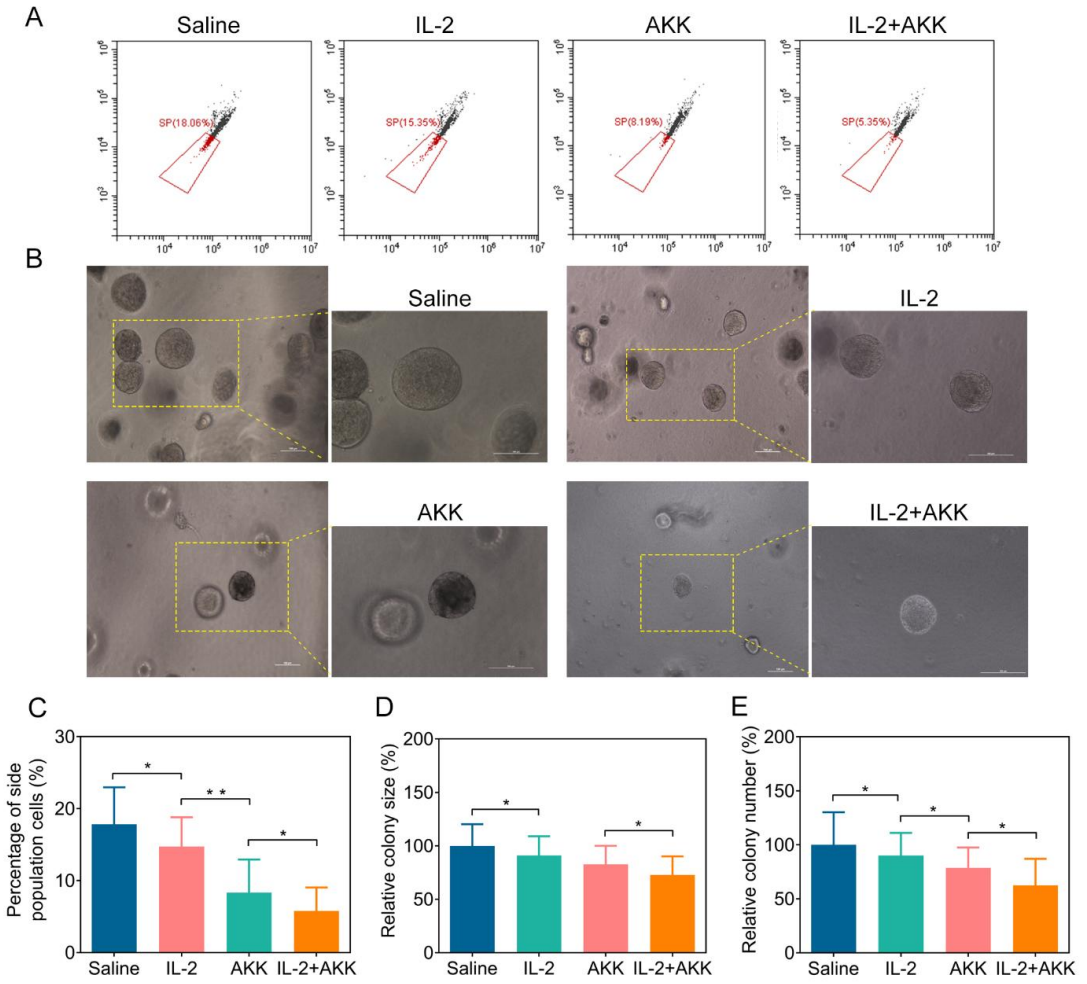

Figure S8. Side population cell analysis and tumor spheroids formation assay of tumor tissues from B16F10 tumor-bearing mice. Single cell suspensions were prepared from the tumor tissues. (A) Representative flow cytometry analysis of side population cells by flow cytometry (x-axis: PB 450-H, y-axis: Violet 660-H). (B) Representative images of spheroids of B16F10 tumor cells cultured in soft 3D fibrin gels (scale bar = 100 μm). The single cell suspensions of tumor tissues were seeded into soft 3D fibrin gels and incubated for 5 days. (C) Percentage of side population cells. (D, E) Relative colony size (D) and number (E) of tumor spheroids on the 5th day after tumor cells were seeded into the soft 3D fibrin gels. All data are shown as mean ± SD (n = 6, **P* < 0.05, ** *P* < 0.01).

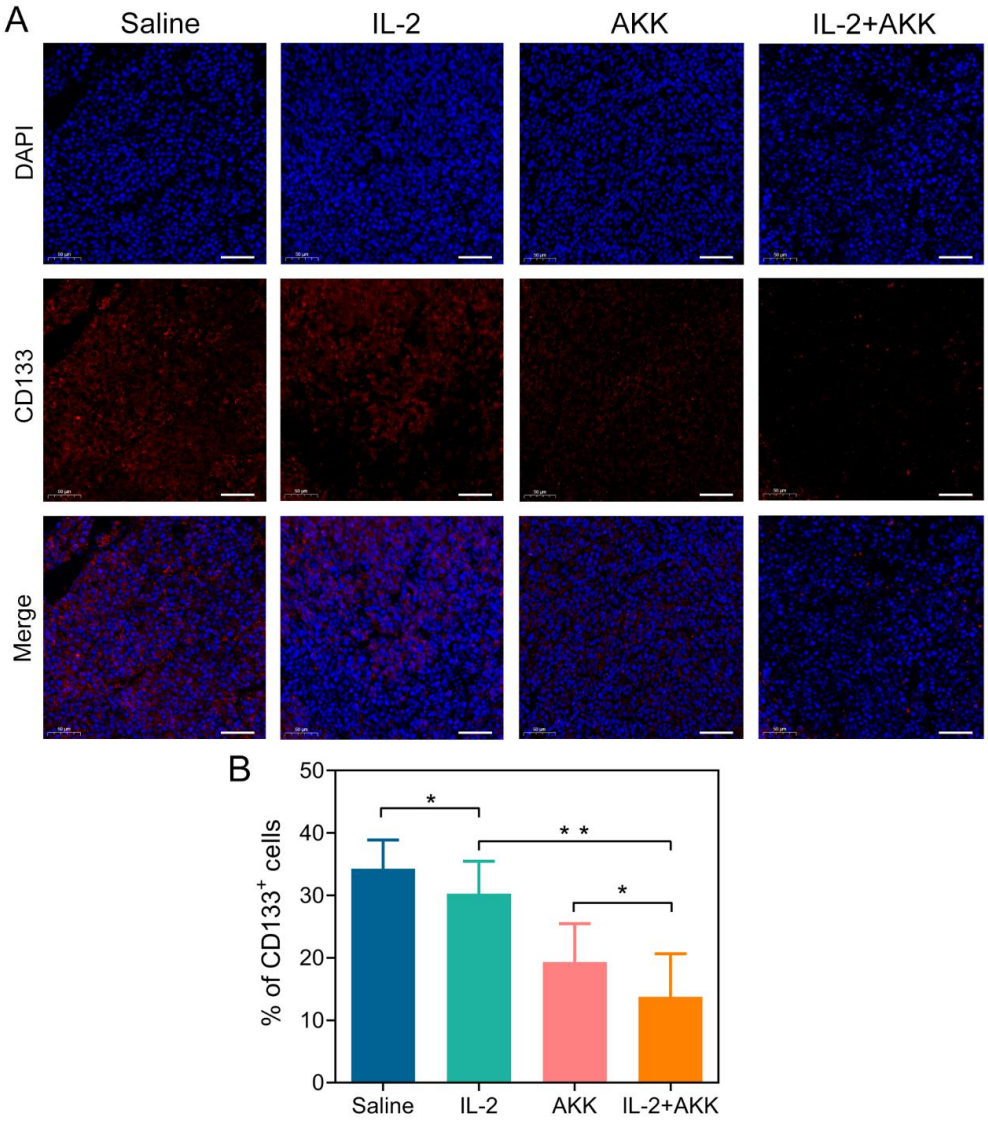

Figure S9. Representative immunofluorescent staining (A) and quantitative analysis (B) of $CD133^+$ cells in the tumor tissues collected from CT26 tumor bearing mice among different treatment groups (200×, scale bar = 50 μm). All data are shown as mean ± SD (n = 6, **P* < 0.05, ** *P* < 0.01).

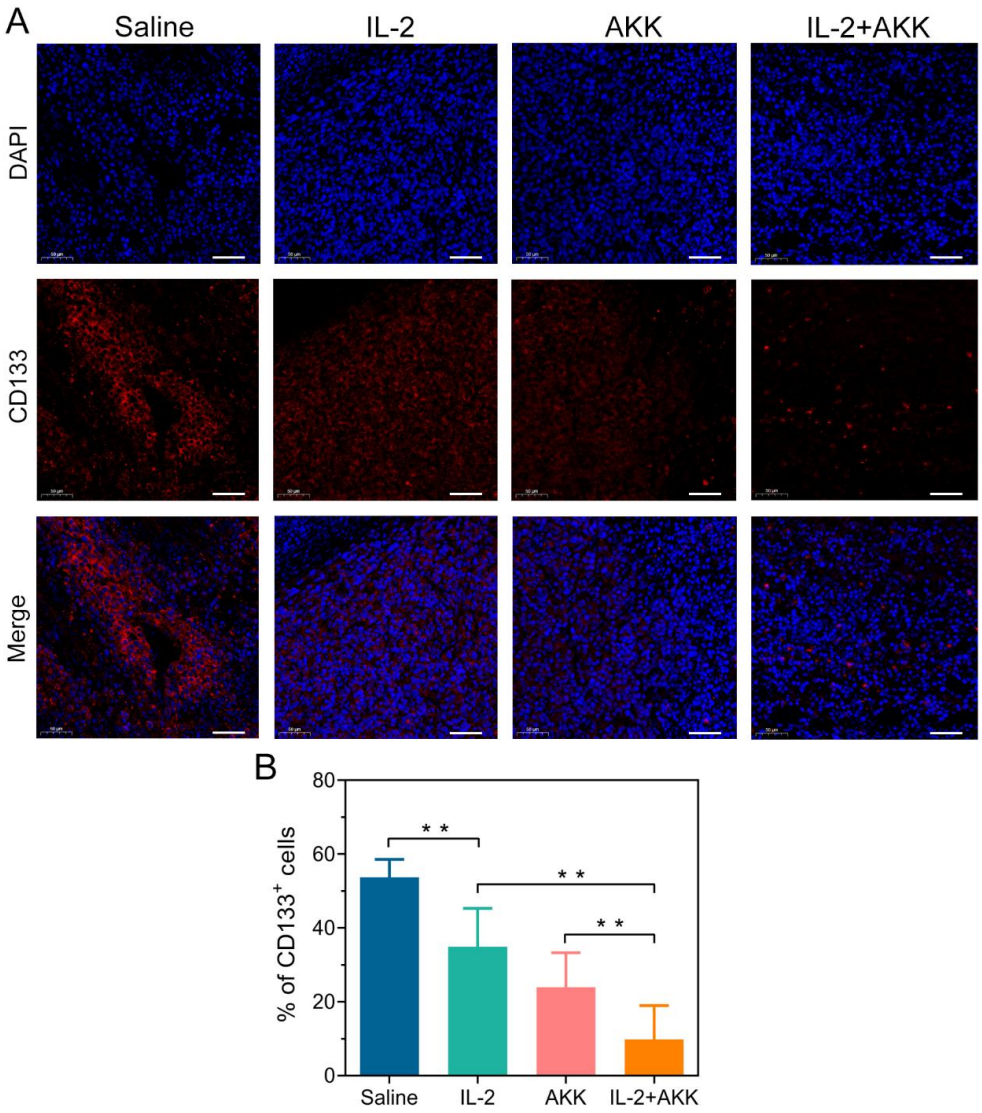

Figure S10. Representative immunofluorescent staining (A) and quantitative analysis (B) of CD133⁺ cells in the tumor tissues collected from B16F10 tumor bearing mice among different treatment groups (200×, scale bar = 50 μm). All data are shown as mean ± SD (n = 6, ** $P < 0.01$).

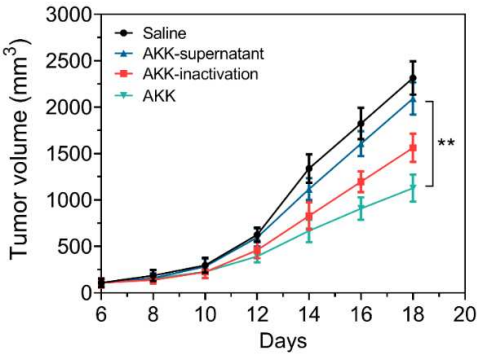

Figure S11. Tumor growth in B16F10 tumor-bearing mice treated with the pasteurized AKK and the culture supernatant of AKK (n = 6). Data are shown as mean ± SD (** $P < 0.01$).

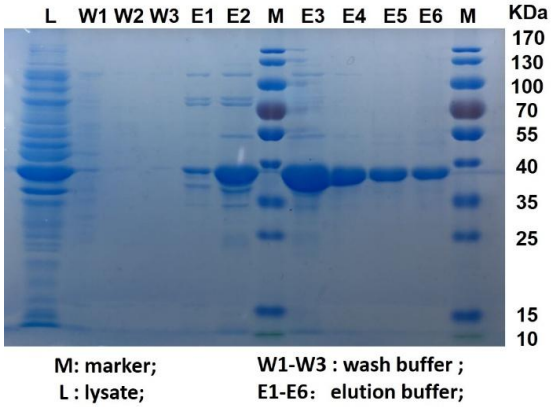

Figure S12. Purification of Amuc. The purification process of Amuc (~40 kDa) was characterized by sodium dodecyl sulfate polyacrylamide gel electrophoresis (SDS-PAGE).

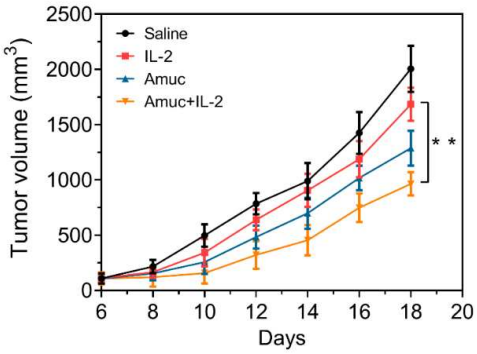

Figure S13. Tumor growth in B16F10 tumor-bearing mice treated with IL-2 and Amuc (n = 6). Data are shown as mean ± SD (** $P < 0.01$).

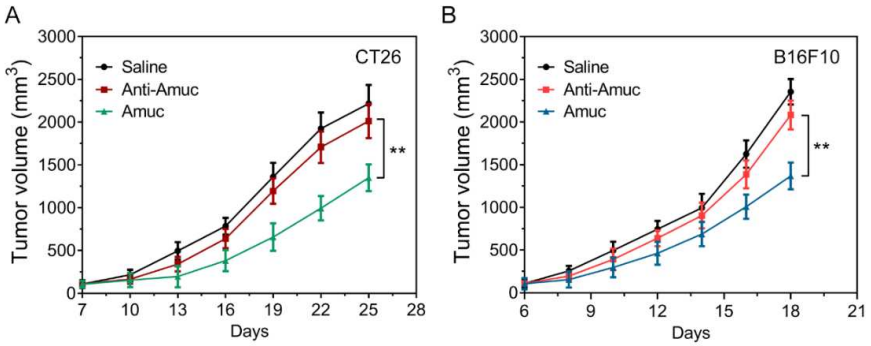

Figure S14. Tumor growth in CT26 tumor-bearing mice (A) or B16F10 tumor-bearing mice (B) treated with blocked Amuc. In the anti-Amuc group, Amuc was pretreated with anti-Amuc antibody before oral delivery to tumor-bearing mice. All data are shown as mean ± SD (n = 6, ** $P < 0.01$).

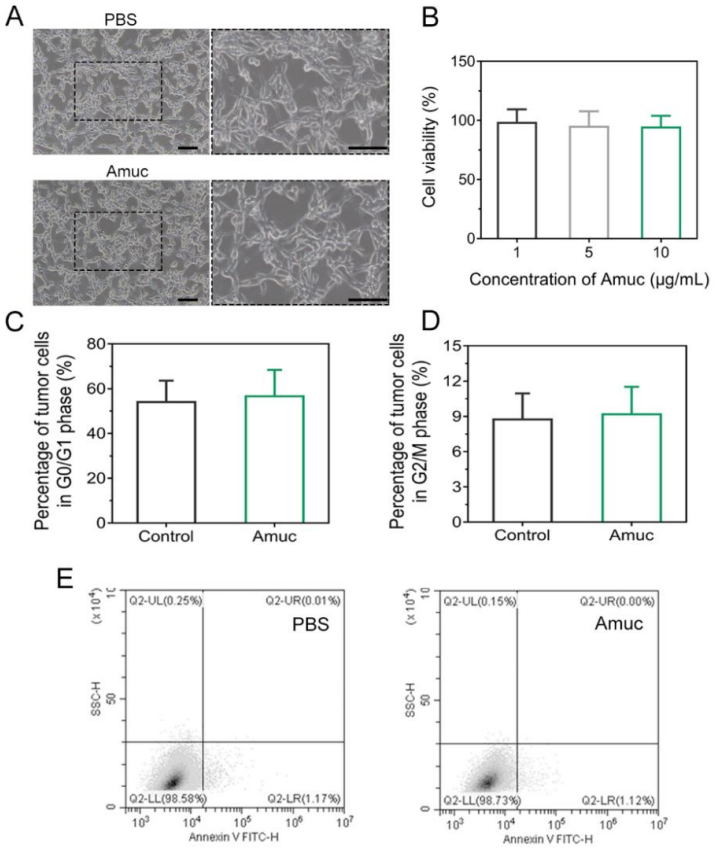

Figure S15. Effects of Amuc on CT26 tumor cells in vitro. (A) Representative images of cell morphology after Amuc treatment (100× or 200× enlargement, scale bar = 100 μm). (B) Cell viability after treatment with different concentration of Amuc for 24 hours. The viability was measured by CCK-8 method (n = 8). (C, D) Cell cycle analysis after receiving Amuc treatment for 24 hours (n = 8). (E) Representative flow cytometry analysis of apoptosis tumor cells after incubation with Amuc for 24 hours**.**

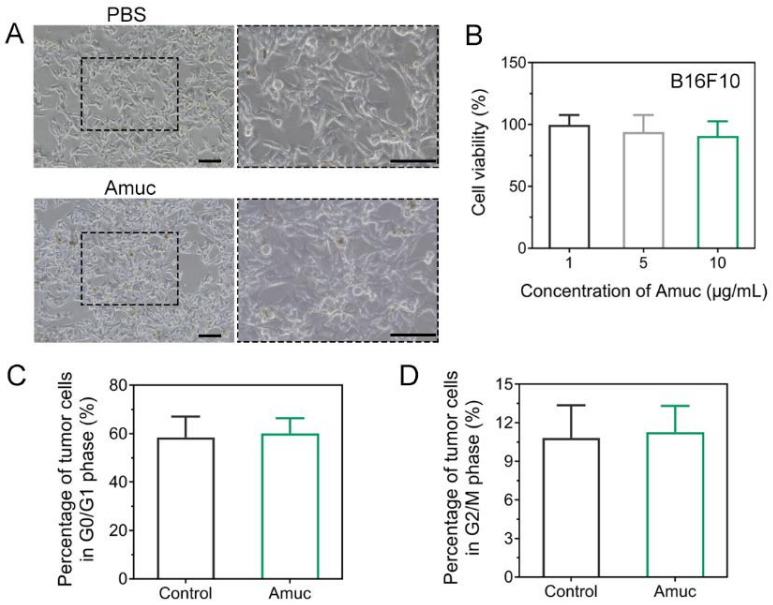

Figure S16. Effects of Amuc on B16F10 tumor cells in vitro. (A) Representative images of cell morphology after Amuc treatment (100× or 200× enlargement, scale bar = 100 μm). (B) Cell viability after treatment with different concentration of Amuc for 24 hours. The viability was measured by CCK-8 method (n = 8). (C, D) Cell cycle analysis after receiving Amuc treatment for 24 hours (n = 8).

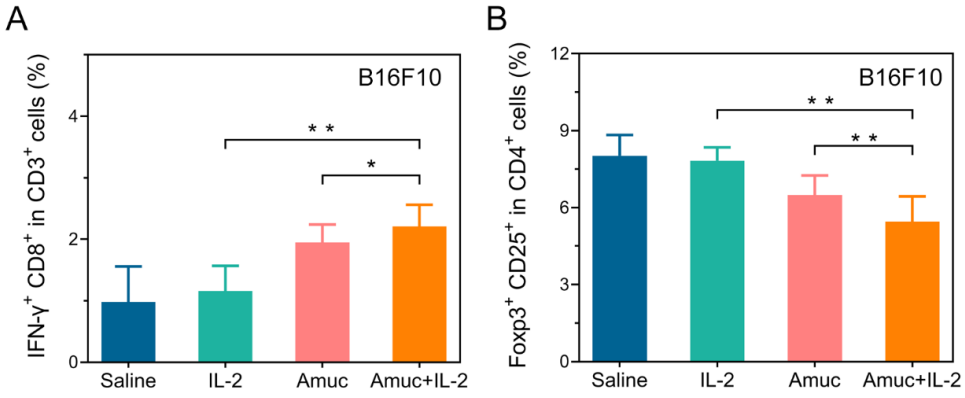

Figure S17. Alterations of tumor immune microenvironment in B16F10 tumor-bearing mice treated with IL-2 and Amuc. (A) Proportions of IFN-γ$^+$ CD8$^+$ in CD3$^+$ T cells in tumor-draining lymph nodes. (B) Proportions of Foxp3$^+$ CD25$^+$ in CD4$^+$ T cells in tumor-draining lymph nodes. Data are shown as mean ± SD (n = 6, *$P < 0.05$, ** $P < 0.01$).

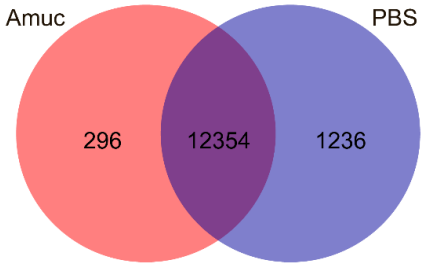

Figure S18. Venn diagram of the identified differentially expressed genes from tumor-infiltrating lymphocytes between Amuc treatment and PBS treatment.

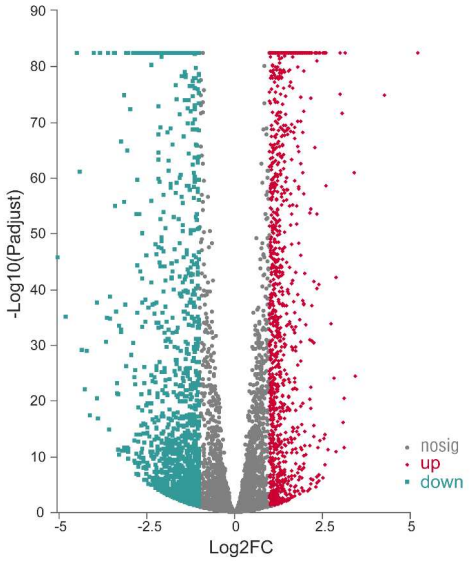

Figure S19. Volcano plots indicating the differentially expressed genes of tumor-infiltrating lymphocytes (Amuc treatment *vs* PBS treatment).

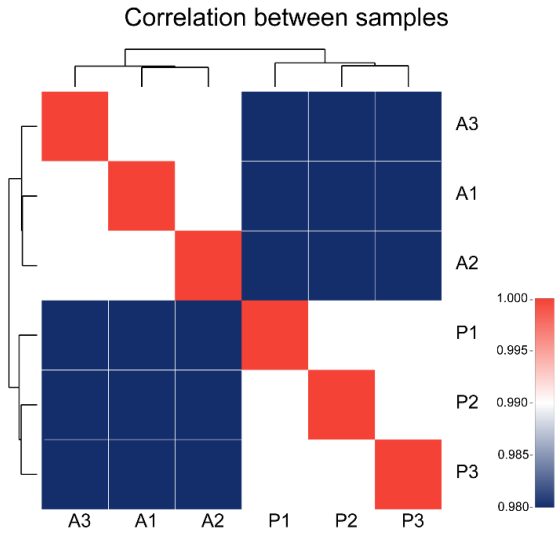

Figure S20. Correlation analysis of the transcriptomic data among different samples (A1-3: Amuc treatment; P1-3: PBS treatment).

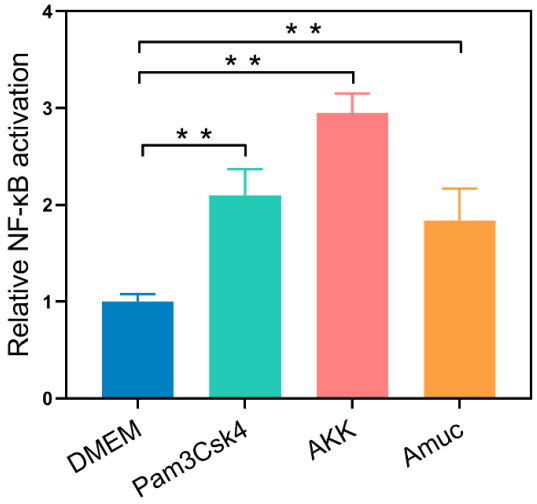

Figure S21. Stimulation effect of AKK and Amuc on TLR2-expressing HEK 293T cells in vitro. Dual-luciferase reporter gene assay for TLR2 was performed in HEK 293T cells after AKK (1×10^7 CFU/mL) or Amuc (10 μg/mL) treatment. Data are shown as mean ± SD (n = 6, **P* < 0.05, ** *P* < 0.01).

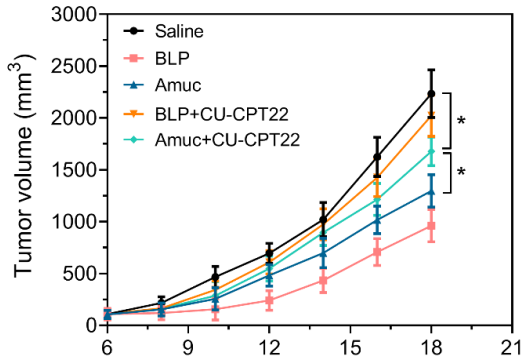

Figure S22. Tumor growth in B16F10 tumor-bearing mice under different treatments (n = 6). The synthetic bacterial lipoprotein (BLP, a TLR1/TLR2 agonist) was used as the positive control and CU-CPT22 (a TLR1/TLR2 antagonist) as the negative control. Data are shown as mean ± SD (*P < 0.05).

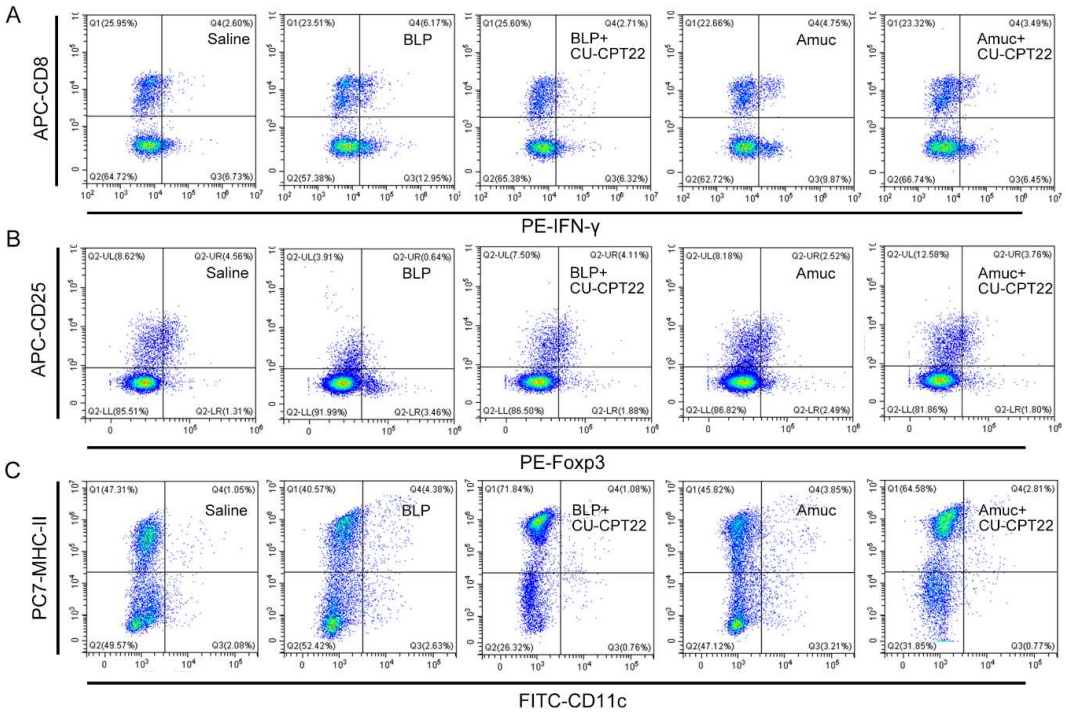

Figure S23. The role of TLR2 pathway in Amuc induced alterations of the tumor immune microenvironment. (A) Representative flow cytometry analysis of cytotoxic effector T cells in tumor-draining lymph nodes (Gated on CD3). (B) Representative flow cytometry analysis of Treg cells in tumor-draining lymph nodes (Gated on CD4). (C) Representative flow cytometry analysis of activated DCs in tumor-draining lymph nodes. Data are representative of the results in both CT26 and B16F10 tumor-bearing mice.

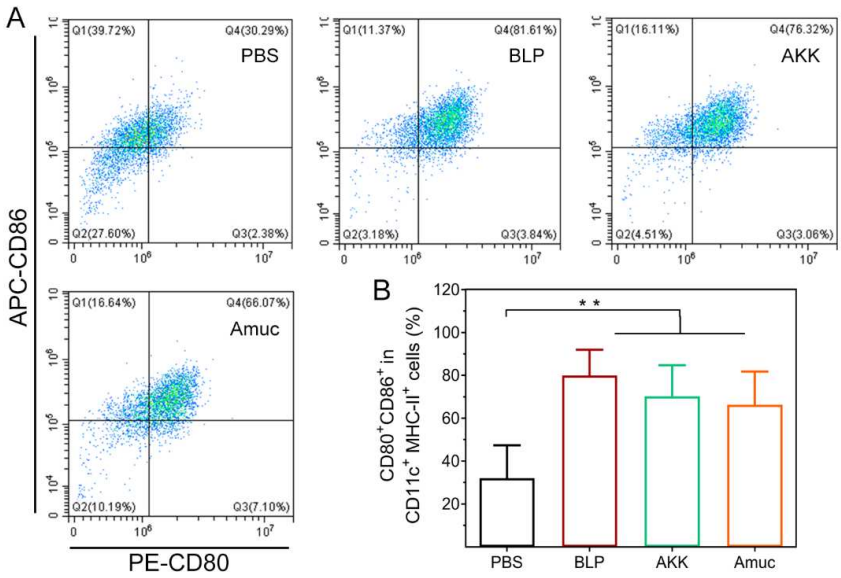

Figure S24. The role of TLR2 pathway in Amuc-induced activation of BMDCs in vitro. BMDCs were incubated with PBS, BLP (5 μg/mL, a TLR1/TLR2 agonist), AKK (1×10^7 CFU/mL) and Amuc (10 μg/mL) for 48 h prior to flow cytometry analysis (n = 6-8). (A) Representative flow cytometry analysis of the activated DCs. (B) Proportions of $CD80^+$ $CD86^+$ in $CD11c^+$ $MHC\text{-}II^+$ cells in BMDCs. Data are shown as mean ± SD (** $P < 0.01$).

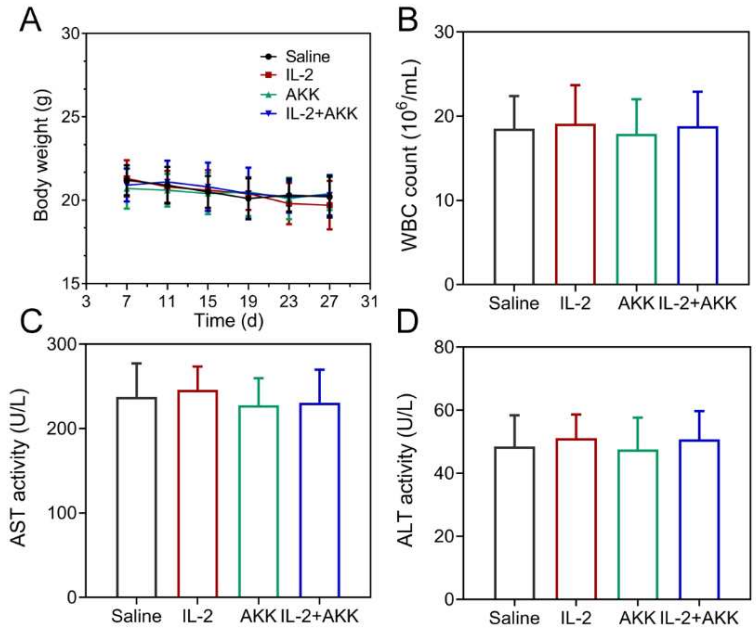

Figure S25. Body weight and blood biochemical analysis in CT26 and B16F10 tumor-bearing mice receiving different treatments (n = 6). Data are representative of the results in both CT26 and B16F10 tumor-bearing mice.

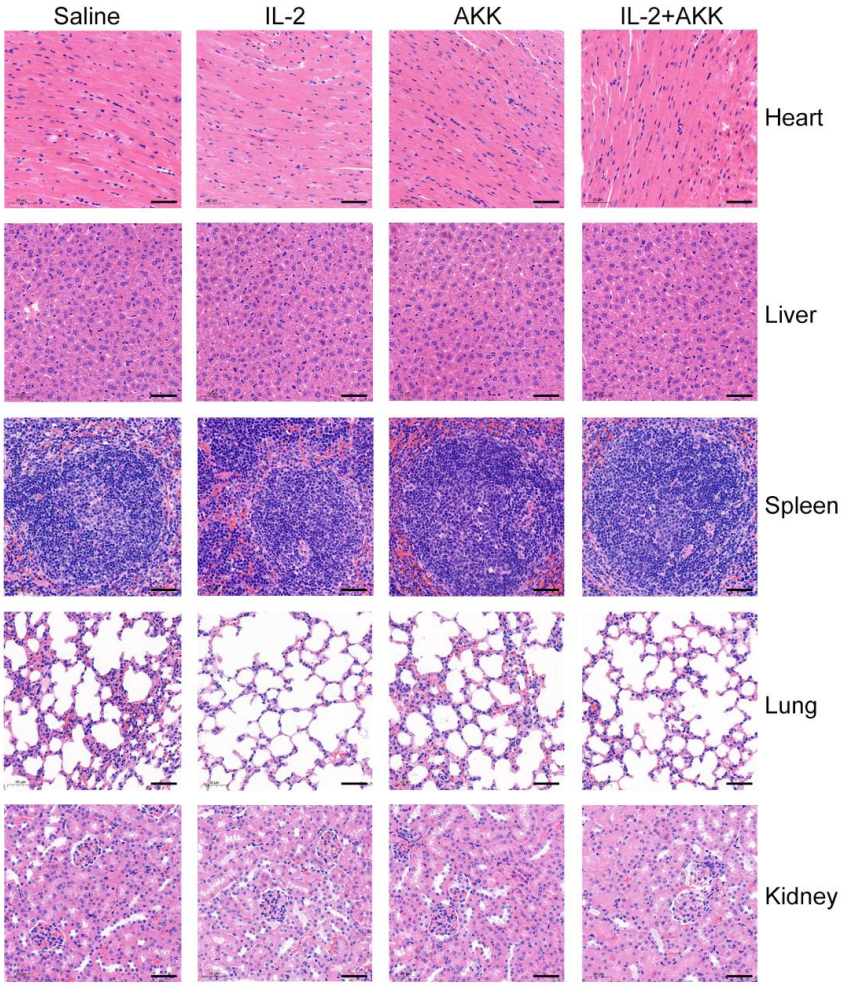

Figure S26. Representative images of H&E staining of tissues from main organs (heart, liver, spleen, lung, and kidney) in CT26 tumor-bearing mice after treatment with IL-2 and AKK (n = 4-6, 200×, scale bar = 50 μm).

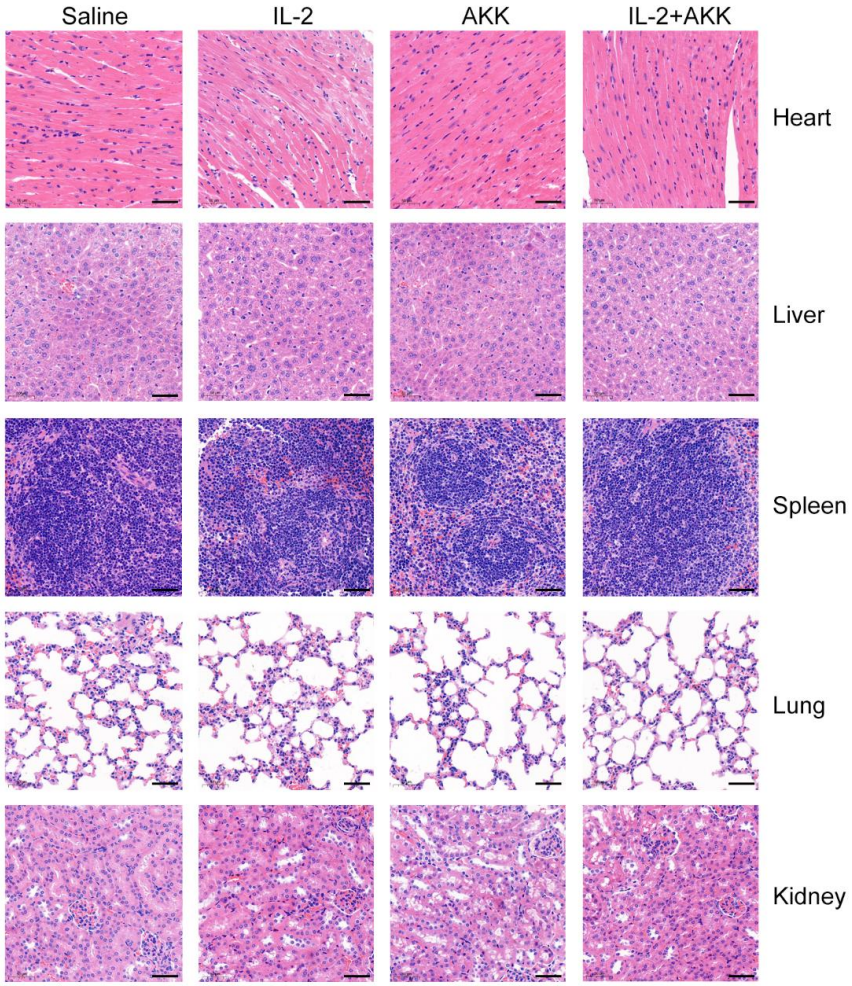

Figure S27. Representative images of H&E staining of tissues from main organs (heart, liver, spleen, lung, and kidney) in B16F10 tumor-bearing mice after treatment with IL-2 and AKK (n = 4-6, 200×, scale bar = 50 μm).

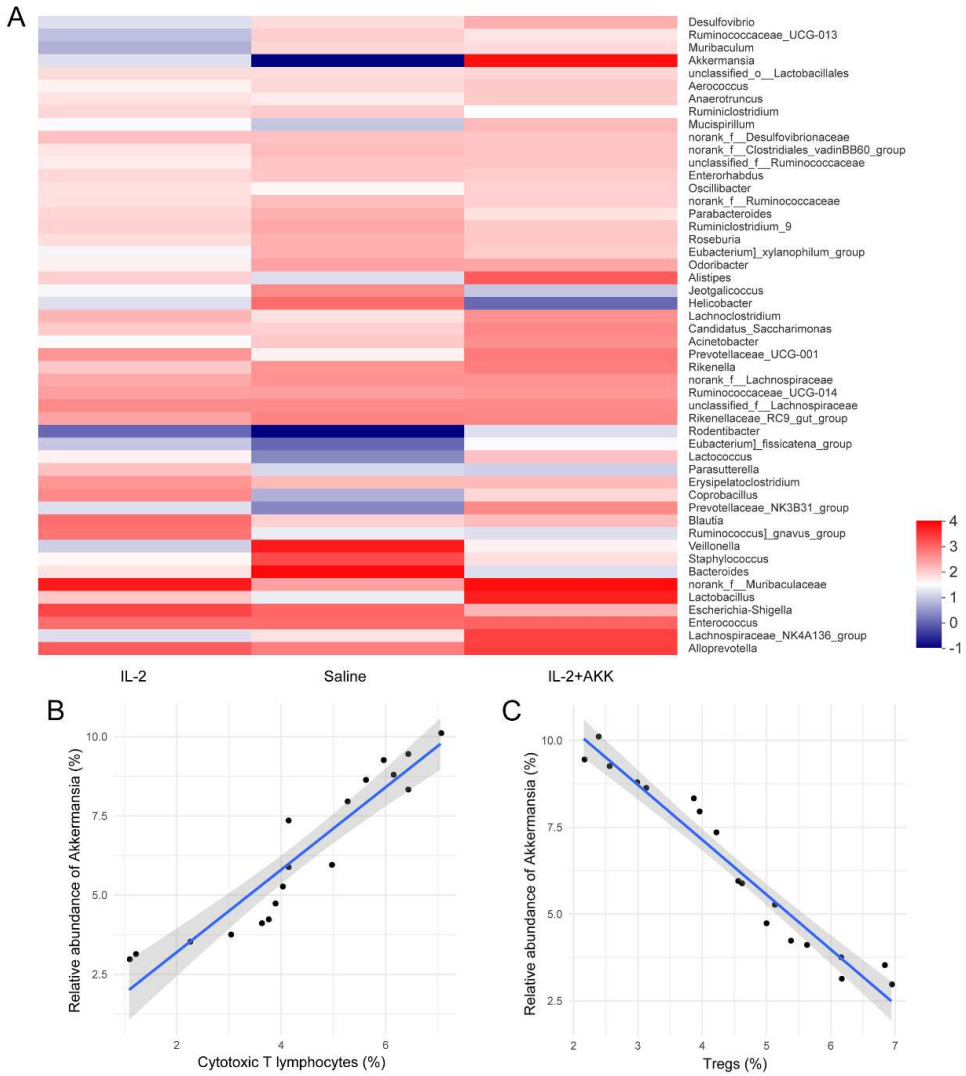

Figure S28. Effects of AKK pretreatment on regulating gut microbiota homeostasis in the context of IL-2 treatment. (A). Community heatmap analysis at the genus level among different treatment groups (n = 6). Color gradient is used to show the variation of bacterial annotation and abundance information among different treatment groups. Correlation analysis between the relative abundance of AKK and the percentage of (B) cytotoxic T cells ($r = 0.9379$, $p < 0.05$) and (C) Tregs ($r = -0.9732$, $p < 0.05$) in tumor-draining lymph nodes among different treatment groups.

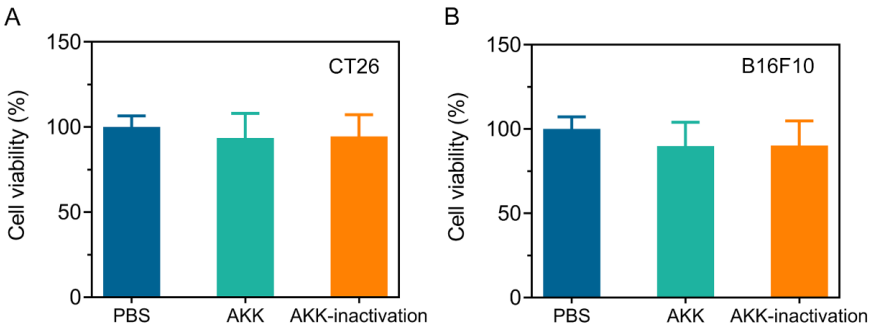

Figure S29. Effects of AKK and pasteurized AKK on CT26 (A) and B16F10 (B) tumor cells in vitro. After treatment with alive AKK (1×10^7 CFU/mL) and pasteurized AKK (an equivalent dose of alive AKK was inactivated by pasteurization at 70 °C for 30 min) for 24 hours. Cell viability was measured by CCK-8 method (n = 8).

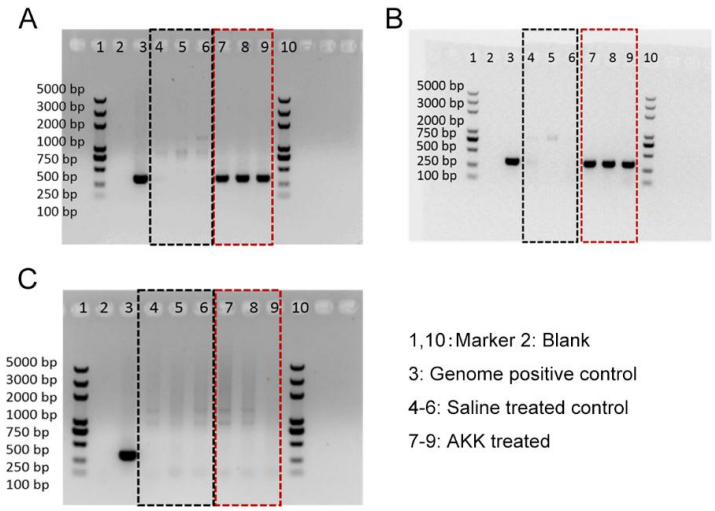

Figure S30. AKK detection in CT26 tumor-bearing mice. DNA was extracted from intestinal content (A), fecal samples (B) and tumor tissues (C), and amplified with AKK specific primers (~320 bp) between tumor-bearing controls and AKK treated group (n = 3).

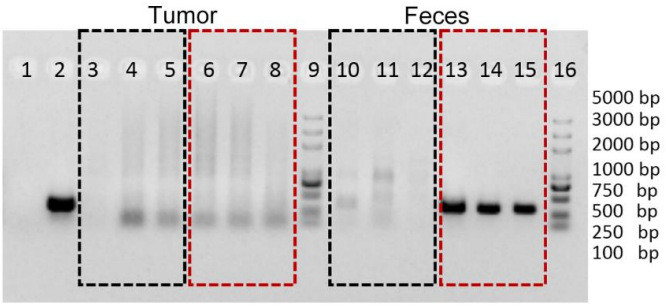

1: Blank 2: Genome positive control 9,16: Marker

3-5: Saline treated control 6-8: AKK treated group

10-12: Saline treated control 13-15: AKK treated group

Figure S31. AKK detection in B16F10 tumor-bearing mice. DNA was extracted from tumor tissues and fecal samples and amplified with AKK specific primers (~320 bp) between tumor-bearing controls and AKK treated group (n = 3).

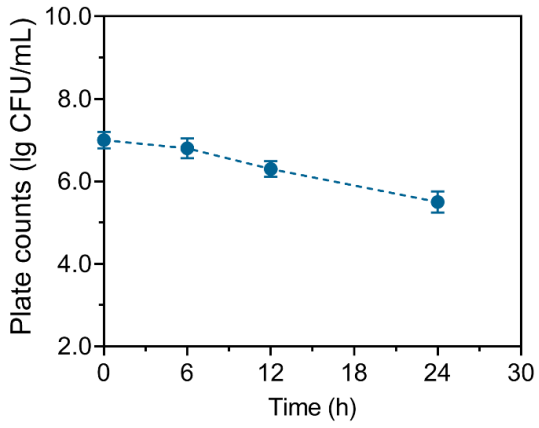

Figure S32. Survival of AKK after exposure to oxygen over time. AKK co-cultured with tumor cells were exposed to ambient air and incubated at 37 °C, which was the same condition as the experiments on CRC patients derived ex-vivo tumor tissues. At predetermined time points over a period of 24 h, the co-culture suspensions were collected and serially diluted 10-fold with PBS. 10 μL aliquots of each dilution were spotted on mucin-based plates. Survival rate of AKK was determined by CFU counts on the plates.

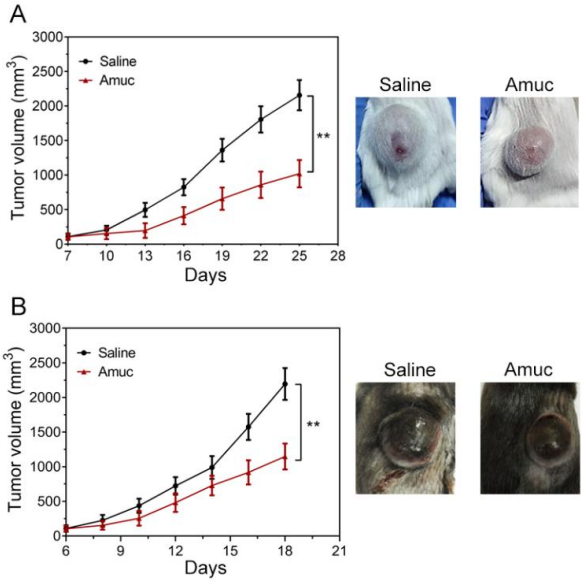

Figure S33. Tumor growth in CT26 (A) or B16F10 (B) tumor-bearing mice treated with in situ injection of Amuc. Data are shown as mean ± SD (n = 6, ** $P < 0.01$).

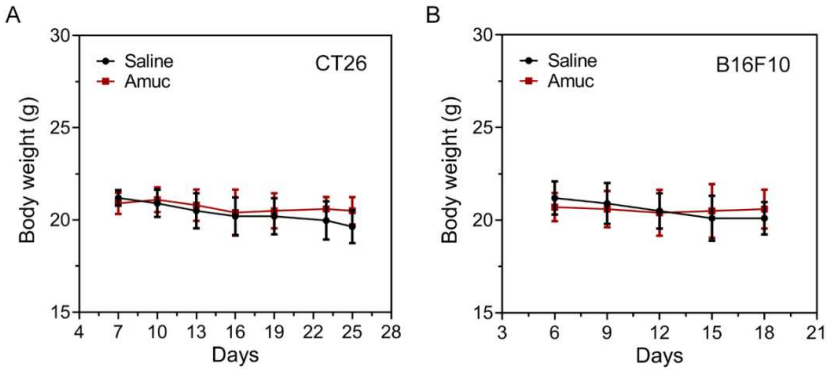

Figure S34. Body weight change of CT26 (A) or B16F10 (B) tumor-bearing mice after in situ injection of Amuc. Data are shown as mean ± SD (n = 6).

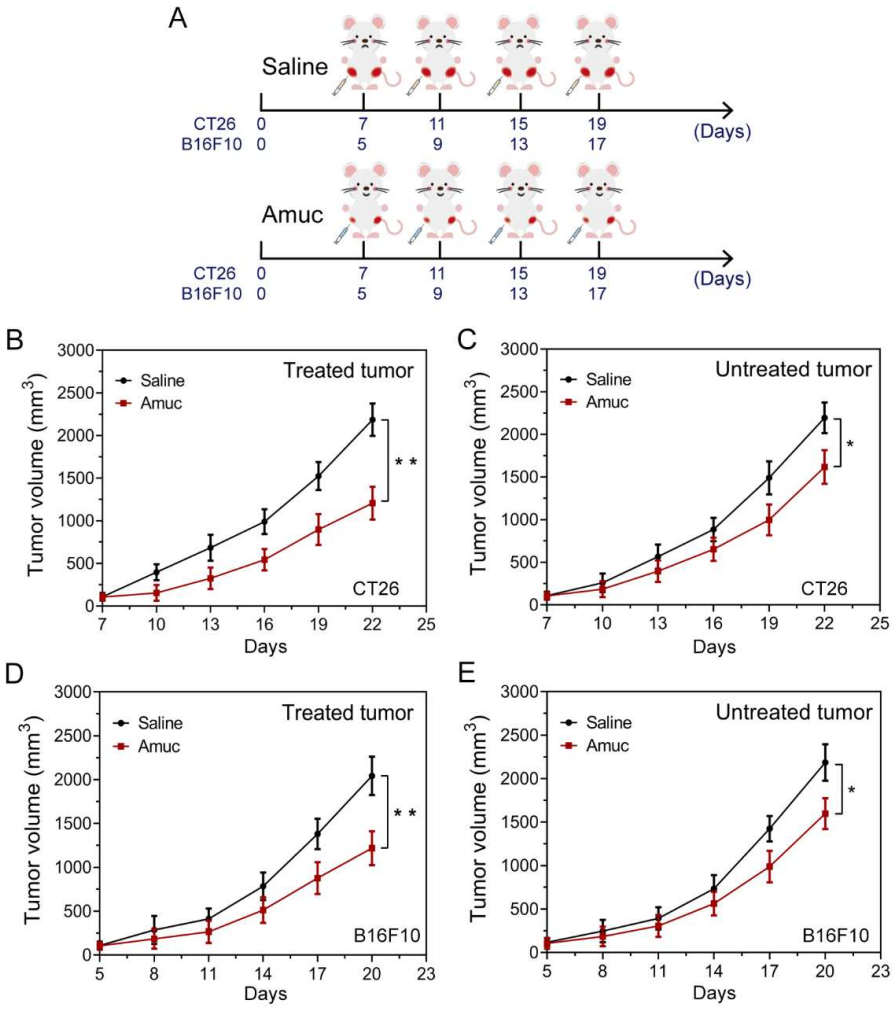

Figure S35. In situ injection of Amuc induces systemic antitumor immune responses in CT26 and B16F10 tumor bearing mice (n = 6). Amuc was injected into one side of the tumors in bilateral tumor models. Saline was injected into the same side in the control group. Tumors on the other side remain untreated in both groups. (A) Experimental scheme of single-flank in situ injection in tumor-bearing mice. (B, C) Tumor growth on the treated side (B) and untreated side (C) in CT26 tumor-bearing mice. (D, E) Tumor growth on the treated side (D) and untreated side (E) in B16F10 tumor-bearing mice. Data are shown as mean ± SD (*$P < 0.05$, ** $P < 0.01$).

Supplementary table 1

Table S1. Clinical Characteristics of the CRC patients.

CRC cases			
Age	66	55	51
Sex	Male	Male	Female
Body mass index	20.6	26.2	25.9
CRC stage	2	3	3
TNM stage	T4N0M0	T4N2M0	T4N2M0
Site of tumor	Sigmoid	Sigmoid	Ascending